NANO LETTERS

pubs.acs.org/NanoLett

Letter

Photonic-Cavity-Enhanced Laser Writing of Color Centers in Diamond

Anchita Addhya, Victor Tyne, Xinghan Guo, Ian N. Hammock, Zixi Li, Melody Leung, Clayton T. DeVault, David D. Awschalom, Nazar Delegan, F. Joseph Heremans, and Alexander A. High*

Cite This: *Nano Lett.* 2024, 24, 11224−11231

Read Online

ACCESS | Metrics & More | Article Recommendations | Supporting Information

ABSTRACT: Color centers in diamond have widespread utility in quantum technologies, but their creation process remains stochastic in nature. Deterministic creation of color centers in device-ready diamond platforms can improve the yield, scalability, and integration. Recent work using pulsed laser excitation has shown impressive progress in deterministically creating defects in bulk diamond. Here, we extend this laser-writing process into nanophotonic devices etched into diamond membranes, including nanopillars and photonic resonators with writing and subsequent readout occurring in situ at cryogenic temperatures. We demonstrate the optically driven creation of carbon vacancy (GR1) and nitrogen vacancy (NV) centers in diamond nanopillars and observe enhanced photoluminescence collection from them. We also fabricate bullseye resonators and leverage their cavity modes to locally amplify the laser-writing field, yielding defect creation with picojoule write-pulse energies 100 times lower than those typically used in bulk diamond demonstrations.

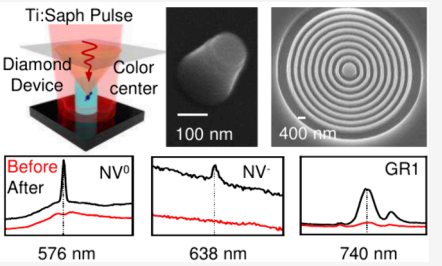

KEYWORDS: *laser writing, diamond nanophotonics, color centers, cavity coupling, bullseye antennas, nanopillars*

Color centers in diamond, such as negatively charged nitrogen vacancy (NV) centers, have excellent spin and optical properties[1] and are widely utilized in quantum sensing[2−5] and networking.[6,7] However, while these technologies would greatly benefit from precise defect localization and controlled optical interfacing, most methods for generating color centers are highly stochastic. Thermal annealing is commonly used to mobilize vacancies, generated by ion or electron bombardment, to combine stochastically with dopants.[8,9] More localized methods, such as masked implantation, enable accurate spatial positioning but lack precise control over the number of color centers at each site.

Recently, laser writing has emerged as an alternative method to generate localized color centers in diamond and other wide-bandgap semiconductors.[10,11] Laser writing utilizes ultrashort high-energy optical pulses to generate hot excitons, which then relax, delivering energy to the lattice locally,[12,13] creating localized vacancies. Most of the existing laser writing work has shown generation of color centers in diamond[14] and SiC[15,16] using wavefront correction[17] and a Solid Immersion Lens (SIL),[14] but with furnace annealing which still results in stochastic distributions. Alternatively, subsequent laser pulses can mobilize the vacancies and encourage binding with substitutional nitrogen in the lattice, resulting in near-unity yield of deterministic NV creation.[18]

Spatially controlled color center generation in photonic devices, commonly used in sensing and networking applications, can improve the yield and scalability of diamond-based quantum technologies. The common approach of fabricating devices around randomly distributed quantum defects is a time-intensive process and exacerbates defect-device coupling errors. Recent attempts to integrate photonics with laser-written defects (e.g., with femtosecond laser-enabled photonic circuit fabrication[19−21]) incur significant signal loss due to detrimental surface modifications.

In this work, we have developed device-integrated laser writing in diamond membranes to simultaneously address the challenges of color center creation, readout, and photonic integration. To ensure that our system can be integrated with a wide array of classical and quantum technologies, we perform laser writing in 300 nm thick diamond membranes, a versatile platform that can be integrated into complex heterogeneous material architectures while maintaining compatibility with coherent color centers,[22] advanced strain engineering, and photonic crystal cavities with record performance.[23,24] The use of a thin-film membrane on thermal oxide wafers also allows us to bypass angled-etch and undercutting processes, which usually result in more complicated procedures, unwanted surface roughness, and polishing-induced thickness variations.[25] Extending laser writing to easily heterogeneously integrable diamond membranes broadens the method's

Received: June 4, 2024
Revised: August 13, 2024
Accepted: August 14, 2024
Published: August 29, 2024

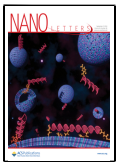

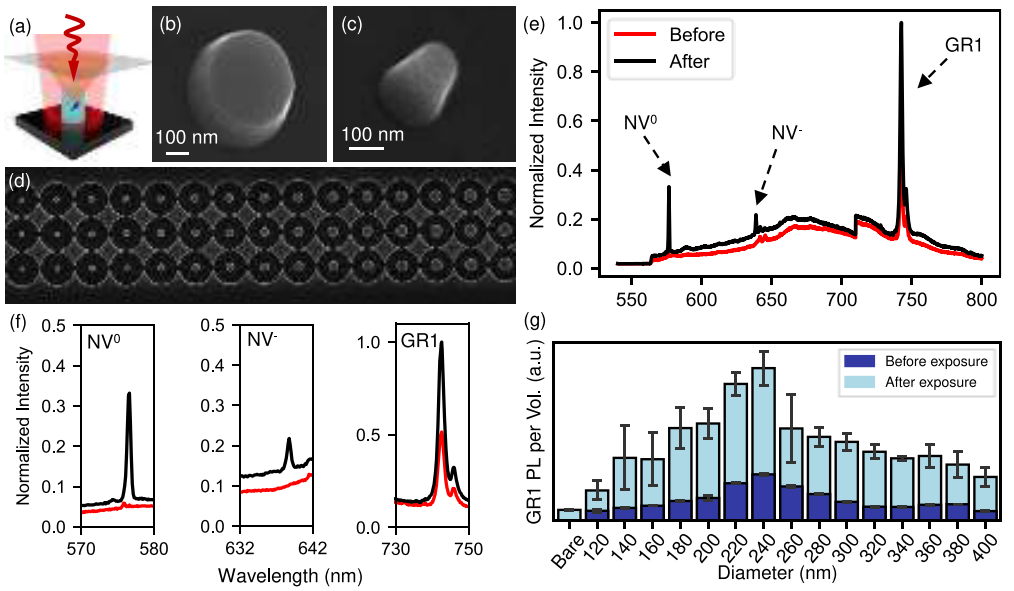

Figure 1. Laser writing in diamond nanopillars. (a) Schematic of a diamond nanopillar sitting on HSQ-covered thermal oxide with a single spin at the center of the pillar emitting into the monitor on top, with pulsed Ti:Saph-excitation for color center creation. (b,c) Angled SEM of 300 nm tall diamond pillars with 400−120 nm diameters. (d) SEM image of a 15 × 3 array of nanopillars. Diameters increase toward the right in steps of 20 nm, starting at 120 nm, with each column containing a set of equal diameters. (e) PL spectra before and after laser irradiation showing creation of color centers (the break in spectra around 710 nm is an artifact of the spectrometer's stitching function). (f) Sharp peaks at 576, 638, and 741 nm indicating creation of NV^0, NV^-, and GR1. (g) Increase in the GR1 PL signal from an array of 45 nanopillars individually irradiated with 408 pJ of pulse energy. The PL signal is normalized to the volume under excitation, determined by the volume of the structure (nanopillars) or the laser spot size (bare membrane).

compatibility with hybrid quantum systems and advanced device architectures.

We leverage the field intensity enhancement in nanophotonic structures, commonly used in quantum technologies, to locally create vacancies and color centers within devices. The field intensity enhancement locally lowers the laser power threshold for vacancy and color center creation. As a result, unlike previous laser writing protocols,[14,17] this method circumvents the need for high-NA objectives, spatial light modulators (SLMs), and SILs and relaxes demands on the laser source, reducing cost and footprint. The use of intensity enhancement to create colocalized color centers opens a pathway toward cavity-confined creation of spin-photon interfaces in which the color center is preferentially created at the cavity field maximum within the cavity-enhanced volume. The nanophotonic devices, including nanopillars and bullseye cavities, can also improve collection efficiency (CE) in comparison with bulk diamond and bare membranes.

We begin by investigating color center creation in nitrogen-implanted diamond nanopillars via pulsed laser irradiation (Figure 1a). Diamond nanopillars are broadly utilized to enhance photon collection from color centers and coupling to biomolecules for quantum sensing applications.[23,26−29] We fabricate nanopillars using e-beam lithography (Methods), enabling the creation of multiple sets of diamond nanopillars with varying diameters. The fabricated nanopillars display surfaces with no discernible signatures of etching trenches (Figure 1b−d), reducing detrimental effects from the fabrication process. Additionally, they showcase improved photon collection efficiency (SI Figure S1) observed from both simulations and PL measurements.

To systematically investigate laser-writing in nanopillars, we use three identical rows of nanopillars with diameters ranging from 120 to 400 nm (Figure 1d). We perform both laser-writing and PL measurements at 4 K to improve the spectral resolution of the zero phonon lines of different color centers and vacancies. We irradiate individual nanopillars for 1 s with 177 fs pulses from a Ti:Saph laser operating at a central wavelength of 750 nm and repetition rate of 76 MHz. Before and after each irradiation, we measured photoluminescence spectra from the pillars under 500 μW excitation with a 519 nm green diode laser (Figure 1e,f). We observe significantly enhanced emission at the zero-phonon wavelengths corresponding to NV^0 and NV^- along with a phonon sideband and fluorescence from the underlying substrate (Figure 1e). With 408 pJ pulse energy, we observe NV formation in 20% (9 out of 45) of the irradiated pillars (SI Figure S7). These created color centers are localized within the cross-sectional volume of the pillar at the ion implantation depth (150 ± 8 nm). Introduction of higher densities of nitrogen dopants in future studies could improve the yield of color centers in each nanopillar.

Postirradiation, we also observe consistent enhancement of GR1 (neutral carbon monovacancies in diamond) photoluminescence with pulse energies of 80 pJ and above. The GR1s initially present from growth and ion implantation processes were used to benchmark the efficiency of the nanopillar antennas as a function of their radius, which displays a trend analogous to simulated CE (SI Figure S1). Figure 1g maps the PL signal amplitude at 741 nm before laser writing from nanopillars of increasing radius, along with the signal enhancement after laser writing. We did not observe any significant correlation between nanopillar radius and PL signal difference.

Next, we improve our control over the laser-writing process by utilizing resonant cavity structures that allow for in situ colocalization with the device. Specifically, we explore bullseye cavities which are capable of intensity enhancement in a small

https://doi.org/10.1021/acs.nanolett.4c02639
Nano Lett. 2024, 24, 11224−11231

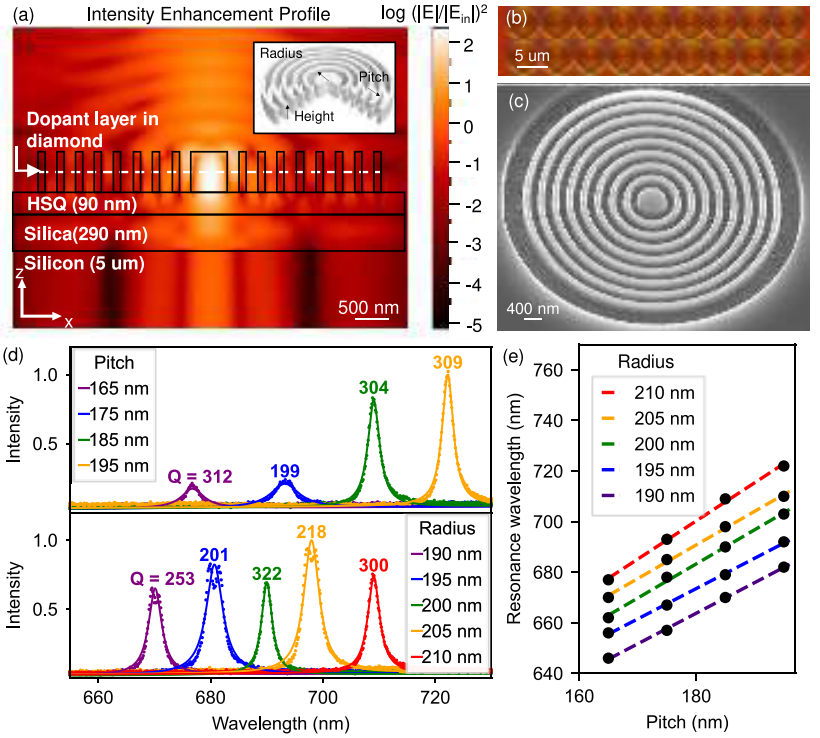

Figure 2. Simulation and experimental characterization of bullseye antennas. (a) Simulated intensity enhancement ($|E/E_{in}|^2$) of an on-resonance bullseye antenna with a Gaussian source at 717 nm obtained by placing a 2D vertical monitor across the center of the bullseye cavity. The implanted layer of dopants is expected to be at 150 nm (marked by a white dashed line). The inset displays a schematic of the cavity labeling the tunable geometric parameters (radius, pitch, and height). (b) Microscope image of a 9 × 3 array of fabricated bullseyes. (c) SEM image of a fabricated bullseye. (d) Background-subtracted PL resonance peaks corresponding to bullseyes with varying pitch with radius fixed at 210 nm (upper panel), varying radius with pitch fixed at 185 nm (lower panel) with their respective quality factors. (e) Linear dependence of resonance wavelength with respect to radius and pitch variation.

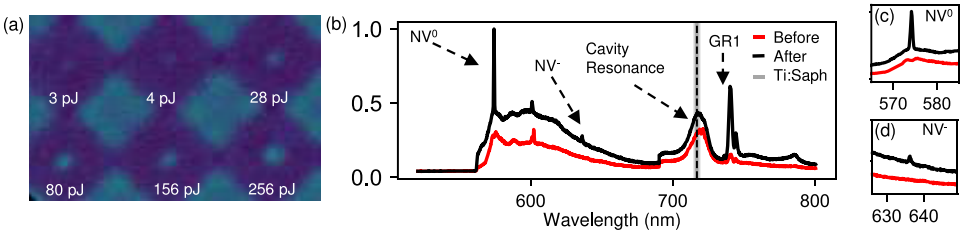

Figure 3. Cavity-coupled creation of color centers in bullseye antennas. (a) PL map of an array of on-resonance bullseye antennas irradiated with 1s Ti:Saph illumination with pulse energies ranging from 3 to 256 pJ. (b) Spectra of GR1s and color centers written in an on-resonance bullseye with 105 pJ of pulse energy with unchanged cavity quality even after irradiation. The Ti:Saph center wavelength is denoted as a dashed line with the fwhm indicated by the shaded region. (c,d) Sharp peaks at 576 and 638 nm indicating creation of NV^0 and NV^-, respectively.

cavity mode, allow straightforward coupling to far-field excitation, and enable efficient photoluminescence collection.[30] Variations of these antennas etched into diamond have already been shown to be a promising avenue for extracting photons from color centers[31] without requiring fine-tuning of spectral overlap with these centers. Additionally, the bullseye cavities' smaller footprints (<5 μm) compared to other resonators result in a compact nanophotonic platform while providing quality factors on the order of 10^2.[32]

The bullseye device comprises a central disk surrounded by concentric rings with a pitch determined by the second-order Bragg condition. Hence their resonances are tunable by varying their radius, pitch, and height (inset of Figure 2a), as seen in finite-difference time-domain (FDTD) simulations (SI Figure S2). To simulate the intensity enhancement for a given wavelength, we tune the geometric parameters and excite them with a Gaussian source. For a fixed structure height of 300 nm, these devices show enhancement of 10^2 times within a mode volume on the order of $\left(\frac{\lambda}{n}\right)^3$, shown in Figure 2a.

We utilized the fabrication process established for diamond nanopillars to fabricate bullseye resonators. After thinning the diamond membrane to the target height, we fabricate an array of bullseyes with variable radius and pitch directly into the diamond (Figure 2b), while keeping the number of rings constant. A scanning electron microscope (SEM) micrograph of an individual bullseye reveals clean structures with smooth sidewalls (Figure 2c). The set of bullseyes reported here covers pitches ranging from 165 to 195 nm and radii ranging from 190 to 210 nm.

To characterize the bullseye cavities, we utilize a 519 nm laser to excite photoluminescence in the underlying HSQ that

https://doi.org/10.1021/acs.nanolett.4c02639
Nano Lett. 2024, 24, 11224−11231

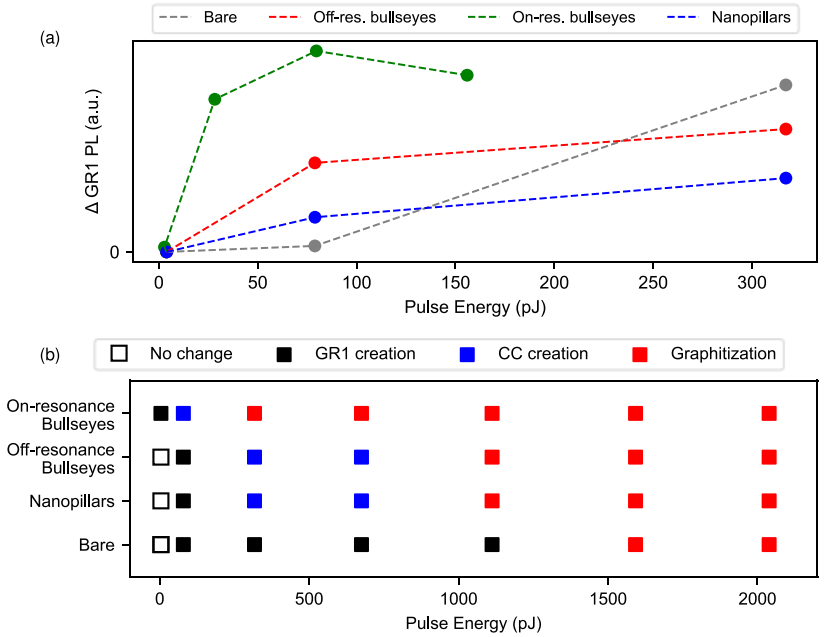

Figure 4. Analysis of laser-induced changes in bare membrane vs in photonic devices. (a) Increase in GR1 counts for increasing pulse energies below the graphitization thresholds, showing an overall dependence on pulse energies and enhancement effects. A higher PL signal is observed for the bare membrane after the initial GR1 creation threshold has been crossed compared to the devices. Higher PL signal detected from GR1s in a bare membrane is attributed to the larger illuminated surface area of the bare membrane. (b) Pulse energy thresholds for laser irradiation on bare membrane vs that in diamond devices. Observed graphitization in on-resonance bullseye antennas occurs at much lower pulse energies than in the bare membrane.

couples to the photonic structure. We observe quality factors between 100 and 300 (a set of which is shown in Figure 2d). Analysis of the entire array of 20 diamond bullseye devices reveals that the resonance wavelengths depend linearly on radius (pitch) when pitch (radius) is kept constant (Figure 2e). This result agrees well with FDTD simulations (SI Figure S2), with a slight red shift (∼17 nm) arising from fabrication imperfections. Precise characterization of these linear relationships provides controlled resonance tuning in the fabrication. This allows for optimized resonant enhancement of the Ti:Saph laser across a broad range of wavelengths and additionally provides an avenue for coresonant outcoupling with a variety of written color centers including silicon-, germanium-, nitrogen-, and tin-vacancy centers.

We utilize arrays of bullseye antennas to investigate cavity-enhanced laser writing. We identify bullseye cavities resonant at 707 ± 2 nm (off-resonance from the Ti:Saph at 717 nm) and irradiate them with incrementally increasing energies ranging from 4 pJ to 2.64 nJ. We observe onset of GR1 creation with 80 pJ pulse energy. To investigate the onset of similar phenomena with on-resonance bullseyes, we utilized an array of antennas resonant at 717 nm. The bullseye antennas designed to be resonant at 717 nm show 160× enhancement according to simulations, with a mode volume of $(240\ \text{nm})^3$ (see Methods). The spectral overlap of the Ti:Saph with an on-resonance antenna is pictorially represented in Figure 3b (further details are shown in SI Figure S10).

We run a fine sweep to identify the thresholds for the on-resonance bullseye antennas with pulse energies ranging from 3 to 256 pJ, since we expect damage to start at significantly lower powers. With increasing irradiation power, the centers of the bullseyes appear brighter in the PL map, indicating formation of optically active defects (Figure 3a). PL spectroscopy before and after laser irradiation shows the controlled formation of color centers in the bullseye (Figure 3b–d). A 57.1% creation efficiency (SI Figure S8) of created color centers (NV^- and/or NV^0) was recorded on irradiating seven identical on-resonance bullseye antennas with 105 pJ of energy. For on-resonance with the Ti:Saph at 717 nm, these antennas leverage high intensity enhancement to lower the required pulse energy. The cavity resonances remain unaffected after laser writing at 105 pJ, reflecting the photonic structures' robustness under laser exposure and their utility for coupling created color centers to external optics.

To quantify the improvement of the creation process in resonators, we perform further analysis of different pulse energy thresholds. We identify critical pulse energies for defect creation in four relevant platforms: a bare (unstructured) membrane, nanopillars, off-resonance bullseyes (detuned to 707 ± 2 nm), and on-resonance bullseyes (Figure 4a). The GR1 creation threshold was observed to be at 4 pJ in on-resonance bullseyes, which is ∼20 times lower than the diamond membrane. This is clear evidence of an intensity-enhanced vacancy creation.

Additionally, for pulse energies greater than 80 pJ, we see a higher GR1 PL signal for the bare membrane in comparison to the nanostructured devices. While the threshold of GR1 creation is a function of resonant enhancement, the number of GR1s formed is a combined function of the resonance and device volume. The illuminated surface area of the bare membrane, equal to the spot size of the laser ($\pi(250\ \text{nm})^2$) is larger than those for the nanopillars ($\pi(120\ \text{nm})^2$) and bullseyes ($\pi(212\ \text{nm})^2$) and is potentially responsible for the higher PL signal detected from GR1s.

To gain further insight, we model the GR1 creation process in the bare membrane (which begins at 80 pJ) by multiphoton ionization (MPI).[33] Fitting the increase in GR1 signal intensity with respect to pulse energy, we observe a trend compatible

https://doi.org/10.1021/acs.nanolett.4c02639
Nano Lett. 2024, 24, 11224−11231

with the MPI model, with the required photon number being 2 (SI Figure S6). This is lower in comparison to previous studies that observed a 9-photon requirement.[17] The lower photon requirement could be due to existing vacancies,[34] proximity to surfaces, and difference in substrate thickness as compared to bulk diamond.

The color center creation itself is a combination of the nonlinear vacancy creation process and subsequent local laser annealing, which causes the vacancy to diffuse within the mode volume of the cavity and combine with a dopant. NV center creation starts at 80 pJ of pulse energy in on-resonance bullseyes compared to 300 pJ in the other types of devices (Figure 4b). Interestingly, there was no color center creation observed in the bare membrane between the GR1 creation and the graphitization threshold within the pulse energies we did measurements at. We anticipate this to be due to the high heat dissipation coefficient of the unstructured diamond membranes, as noted for diamond and SiC in Morelli's[35] and Anufriev's works,[36] resulting in the GR1 vacancies remaining below their thermal mobilization threshold. Decoupling the creation and annealing pulses and varying the parameters of each would allow for a further in-depth understanding of the effect of pulse energy on the yield.

We also characterize the graphitization threshold for each platform, in which visible damage is observed with optical microscopy and confirmed through PL mapping and scanning electron microscopy (SEM) imaging (SI Figure S11). Onset of damage begins in bare membranes at 1.6 nJ, an order of magnitude lower than the graphitization threshold for bulk diamond.[37] The lower damage threshold may be attributed to the MHz repetition rate of the Ti:Saph as compared to previous works that used kHz lasers[38] and the reduced heat dissipation in case of the membranes affixed to glass substrates compared to bulk.[23] Further, we observe a device-dependent reduction of graphitization pulse energy (Figure 4b). This effect is strongest for on-resonance bullseyes, with damage starting at energies as low as 300 pJ due to intensity enhancement within the cavity mode. For lower pulse energy sweeps, we find that GR1 and color center creation thresholds follow a similar platform-dependent trend.

In summary, we established an efficient laser-writing pathway to create colocalized color centers within nanophotonic devices in a diamond membrane using picojoules of pulse energies. Compared to bulk diamond, we have shown a 2 orders of magnitude reduction in pulse energies required to create these solid-state qubits. Utilizing a simple fabrication method to create devices ranging from nanometer to μm scale, our process points toward a scalable photonics platform with integrated color centers and vacancies. We demonstrated a repeatable process for device-aligned color centers with potential use in colocalizing sensing targets for improved sensing[39] and significantly expediting the process of device integration with color centers. Future work will integrate real-time monitoring of the photoluminesnce[18] to enable fully deterministic, spatially localized creation of color centers in nanophotonic devices for hybrid quantum architectures[40] especially utilized for sensing[41,42] and communication.[43] With further improvement in surface processing and laser-writing techniques,[44] we can reliably use this as a viable avenue to establish solid-state quantum protocols. While this work focuses on the NV^- center in diamond, the method presented can be applied to other material systems.[34,45] Future studies could examine laser-driven creation of Group IV color centers, such as tin, silicon, and germanium vacancy centers, in coresonant structures.[32] We also expect plasmonic cavities to have better mode confinement (i.e., subdiffraction limited mode volumes) which can potentially lead to improved localization. A combination of laser writing and masked implantation can further tighten the spatial precision. By improving both the formation and efficiency of color centers, this technique could serve as a reliable avenue to create device-aligned spin qubits and establish a viable pathway toward scalable solid-state quantum platforms.

METHODS

Sample Preparation. The 200 μm × 200 μm diamond membranes were transferred on thermal oxide chips via the smart-cut approach.[22] The samples were then sent out to be ion implanted with $^{14}N^+$ ions at a 7° angle with a dose concentration of 10^{11} ions/cm^2 at 136 keV energies to ensure implantation at 150 nm depth. No annealing was performed.

Simulation. We performed all of our simulations with Lumerical's FDTD module. For Figure 2a, the source type was set to a Gaussian in the backward z-direction propagating toward the sample, focused by a lens of NA 0.85 (experimentally matched) with a radius of 4 μm and a polarization of 0° and the boundary conditions were set to Perfectly Matched Layer (PML). In order to obtain the intensity enhancement of the bullseye antenna, a 2D vertical (XZ) monitor was placed along the central cross-section of the bullseye antenna.

For the mode-volume calculation, we used a bullseye antenna with a radius of 212 nm and a pitch of 207 nm (resonant at 717 nm) placed with a 3D mode volume monitor (800 nm × 800 nm × 300 nm) at the center of the bullseye cavity and used a 717 nm source to excite the mode. The calculation was done using the formula $\frac{\int \epsilon E^2 dV}{\max(\epsilon E^2)}$.

Fabrication. The diamond membranes were transferred onto thermal oxide chips and bonded with HSQ. We thinned the membranes down to the desired height, which in this case was 300 nm. Followed by a generic cleaning process (acetone, IPA, and water), we deposited a 30 nm alumina hard mask using the atomic layer deposition method (Savannah Thermal ALD, Veeco). The process started with a 90 nm electron beam resist deposition (ARP6200.04, MicroChem), followed by a 20 nm gold deposition by thermal evaporation (Nexdep PVD platform, Angstrom Engineering) to prevent charging effects. Cavity patterns were lithographically defined at a dose of 250 μC/cm^2 at 100 keV (Raith EBPG5000 plus), and the gold layer was removed by TFA gold etchant (Transene) afterward. Exposed patterns were developed in amyl acetate for 30 s, followed by 2 rounds of 30 s of IPA stopper and 60 s of DI water rinse. A 30 s ICP RIE etching was then carried out to transfer the pattern into the alumina hard mask. This was followed by resist removal in heated N-methyl-2-pyrrolidone (NMP) at 80 °C. Using the patterned alumina mask, we conducted another round of ICP RIE etching in 30 s intervals until the diamond was etched all the way through. A 20 s dip into aluminum etchant (Type A, Transene) was performed between each etch step to restrict micromasking. A final diacid boil (sulfuric + nic acid) at 225 °C was performed to remove the alumina hard mask as well as surface termination. This yielded diamond nanopillars and bull-eye cavities with spectral tunability. The schematic for the fabrication process is provided in SI Figure S12.

https://doi.org/10.1021/acs.nanolett.4c02639
Nano Lett. 2024, 24, 11224−11231

Measurement. We cooled the sample inside a Montana cryostat to 4 K and characterized the diamond bullseye cavities using a home-built reflection spectroscopy setup with a broadband supercontinuum laser (430−2400 nm, SC-OEM YSL Photonics) and a spectrometer (300 g/mm, Princeton Instruments). Following this, a PL map was recorded using a green diode laser (Thorlabs) emitting at 519 nm and an Excelitas APD. The PL map gives us a confirmed signature of the background emission of the HSQ amplified by the photonic devices. Once the resonance of the cavity was confirmed to be at the target wavelength in the case of the bullseyes, we tuned the Ti:Saph ultrafast pulsed laser source to overlap with the resonance wavelength of the bullseye devices. We ensured mode locking with an autocorrelator (APE) and characterized the pulse energy by measuring the average power with a power meter. We tuned pulse energy with a half-waveplate (Thorlabs). The sample was then irradiated with a series of 177 fs pulses for vacancy and color center creation. The pulse energies used for defining the threshold of the devices (in Figure 4b) were 4, 80, 317, 675, 1112, 1592, 2400, and 2640 pJ. We additionally explored 4, 28, 80, and 105 pJ for on-resonance bullseyes since they displayed signs of GR1 creation at 4 pJ pulse energy (not prevalent in the other devices).The irradiation time, and thus the number of pulses, was controlled by the opening and closing of an optical shutter (Thorlabs) and a flipper motor mirror (Thorlabs) mediating the path of the Ti:Saph to the sample (Figure S5). The devices were then recharacterized via the PL spectroscopy process described above, featuring signals from laser-written color centers. A prominent peak at 741 nm indicated the significant creation of GR1 centers. The peaks at 575 and 637 nm signify the creation of NV^0 and NV^-, respectively.

■ ASSOCIATED CONTENT

Supporting Information

The Supporting Information is available free of charge at https://pubs.acs.org/doi/10.1021/acs.nanolett.4c02639.

Additional details of FDTD simulations, optical setup, characterization and fit methods, statistics of color center creation and fabrication process (PDF)

■ AUTHOR INFORMATION

Corresponding Author

Alexander A. High − *Pritzker School of Molecular Engineering, University of Chicago, Chicago, Illinois 60637, United States; Center for Molecular Engineering and Materials Science Division, Argonne National Laboratory, Lemont, Illinois 60439, United States*; Email: ahigh@uchicago.edu

Authors

Anchita Addhya − *Pritzker School of Molecular Engineering, University of Chicago, Chicago, Illinois 60637, United States*; orcid.org/0009-0007-2443-3926

Victor Tyne − *Department of Physics, University of Chicago, Chicago, Illinois 60637, United States*

Xinghan Guo − *Pritzker School of Molecular Engineering, University of Chicago, Chicago, Illinois 60637, United States*; orcid.org/0000-0003-3896-8765

Ian N. Hammock − *Pritzker School of Molecular Engineering, University of Chicago, Chicago, Illinois 60637, United States*

Zixi Li − *Pritzker School of Molecular Engineering, University of Chicago, Chicago, Illinois 60637, United States*

Melody Leung − *Pritzker School of Molecular Engineering, University of Chicago, Chicago, Illinois 60637, United States*

Clayton T. DeVault − *Pritzker School of Molecular Engineering, University of Chicago, Chicago, Illinois 60637, United States; Center for Molecular Engineering and Materials Science Division, Argonne National Laboratory, Lemont, Illinois 60439, United States*; orcid.org/0000-0001-9544-5384

David D. Awschalom − *Pritzker School of Molecular Engineering, University of Chicago, Chicago, Illinois 60637, United States; Department of Physics, University of Chicago, Chicago, Illinois 60637, United States; Center for Molecular Engineering and Materials Science Division, Argonne National Laboratory, Lemont, Illinois 60439, United States*; orcid.org/0000-0002-8591-2687

Nazar Delegan − *Pritzker School of Molecular Engineering, University of Chicago, Chicago, Illinois 60637, United States; Center for Molecular Engineering and Materials Science Division, Argonne National Laboratory, Lemont, Illinois 60439, United States*

F. Joseph Heremans − *Pritzker School of Molecular Engineering, University of Chicago, Chicago, Illinois 60637, United States; Center for Molecular Engineering and Materials Science Division, Argonne National Laboratory, Lemont, Illinois 60439, United States*; orcid.org/0000-0003-3337-7958

Complete contact information is available at: https://pubs.acs.org/10.1021/acs.nanolett.4c02639

Notes

The authors declare the following competing financial interest(s): A.A.H., A.A., V.T., and F.J.H. have filed a provisional patent (US Patent Appl. No. 63/658,197) for the methods of photonic-enhanced vacancy creation.

■ ACKNOWLEDGMENTS

This work was primarily funded through Q-NEXT, supported by the U.S. Department of Energy, Office of Science, National Quantum Information Science Research Centers. Growth related efforts were supported by the U.S. Department of Energy, Office of Basic Energy Sciences, Materials Science and Engineering Division (N.D.). This work made use of the Pritzker Nanofabrication Facility (Soft and Hybrid Nanotechnology Experimental Resource, NSF ECCS-2025633) and the Materials Research Science and Engineering Center (NSF DMR-2011854) at the University of Chicago. Work performed at the Center for Nanoscale Materials, a U.S. Department of Energy Office of Science User Facility, was supported by the U.S. DOE, Office of Basic Energy Sciences, under Contract No. DE-AC02-06CH11357. The quantum photonics work and part of the membrane bonding work were supported by the Quantum Leap Challenge Institute for Hybrid Quantum Architectures and Networks (HQAN) (NSF OMA-2016136) and NSF award AM-2240399. A.A. additionally acknowledges support from a Kadanoff−Rice fellowship (NSF DMR-2011854). C.T.D. receives support from the CQE IBM postdoctoral fellowship training program. The authors thank Peter Duda for nanofabrication assistance.

REFERENCES

(1) Wolfowicz, G.; Heremans, F. J.; Anderson, C. P.; Kanai, S.; Seo, H.; Gali, A.; Galli, G.; Awschalom, D. D. Quantum guidelines for solid-state spin defects. *Nature Reviews Materials* **2021**, *6*, 906−925.

(2) Maze, J. R.; Stanwix, P. L.; Hodges, J. S.; Hong, S.; Taylor, J. M.; Cappellaro, P.; Jiang, L.; Dutt, M. G.; Togan, E.; Zibrov, A.; et al. Nanoscale magnetic sensing with an individual electronic spin in diamond. *Nature* **2008**, *455*, 644−647.

(3) Choi, J.; Zhou, H.; Landig, R.; Wu, H.-Y.; Yu, X.; Von Stetina, S. E.; Kucsko, G.; Mango, S. E.; Needleman, D. J.; Samuel, A. D.; et al. Probing and manipulating embryogenesis via nanoscale thermometry and temperature control. *Proc. Natl. Acad. Sci. U. S. A.* **2020**, *117*, 14636−14641.

(4) Schirhagl, R.; Chang, K.; Loretz, M.; Degen, C. L. Nitrogen-vacancy centers in diamond: nanoscale sensors for physics and biology. *Annu. Rev. Phys. Chem.* **2014**, *65*, 83−105.

(5) Barry, J. F.; Schloss, J. M.; Bauch, E.; Turner, M. J.; Hart, C. A.; Pham, L. M.; Walsworth, R. L. Sensitivity optimization for NV-diamond magnetometry. *Rev. Mod. Phys.* **2020**, *92*, 015004.

(6) Bernien, H.; Hensen, B.; Pfaff, W.; Koolstra, G.; Blok, M. S.; Robledo, L.; Taminiau, T. H.; Markham, M.; Twitchen, D. J.; Childress, L.; et al. Heralded entanglement between solid-state qubits separated by three metres. *Nature* **2013**, *497*, 86−90.

(7) Pompili, M.; Hermans, S. L.; Baier, S.; Beukers, H. K.; Humphreys, P. C.; Schouten, R. N.; Vermeulen, R. F.; Tiggelman, M. J.; dos Santos Martins, L.; Dirkse, B.; et al. Realization of a multinode quantum network of remote solid-state qubits. *Science* **2021**, *372*, 259−264.

(8) Haque, A.; Sumaiya, S. An overview on the formation and processing of nitrogen-vacancy photonic centers in diamond by ion implantation. *Journal of Manufacturing and Materials Processing* **2017**, *1*, 6.

(9) Toyli, D. M.; Weis, C. D.; Fuchs, G. D.; Schenkel, T.; Awschalom, D. D. Chip-scale nanofabrication of single spins and spin arrays in diamond. *Nano Lett.* **2010**, *10*, 3168−3172.

(10) Liu, Y.; Chen, G.; Song, M.; Ci, X.; Wu, B.; Wu, E.; Zeng, H. Fabrication of nitrogen vacancy color centers by femtosecond pulse laser illumination. *Opt. Express* **2013**, *21*, 12843−12848.

(11) Hadden, J.; Bharadwaj, V.; Sotillo, B.; Rampini, S.; Osellame, R.; Witmer, J.; Jayakumar, H.; Fernandez, T.; Chiappini, A.; Armellini, C.; et al. Integrated waveguides and deterministically positioned nitrogen vacancy centers in diamond created by femtosecond laser writing. *Optics letters* **2018**, *43*, 3586−3589.

(12) Smith, J. M.; Meynell, S. A.; Bleszynski Jayich, A. C.; Meijer, J. Colour centre generation in diamond for quantum technologies. *Nanophotonics* **2019**, *8*, 1889−1906.

(13) Vainos, N. A. *Laser growth and processing of photonic devices*; Elsevier: 2012.

(14) Yurgens, V.; Zuber, J. A.; Flagan, S.; De Luca, M.; Shields, B. J.; Zardo, I.; Maletinsky, P.; Warburton, R. J.; Jakubczyk, T. Low-charge-noise nitrogen-vacancy centers in diamond created using laser writing with a solid-immersion lens. *ACS Photonics* **2021**, *8*, 1726−1734.

(15) Chen, Y.-C.; Salter, P. S.; Niethammer, M.; Widmann, M.; Kaiser, F.; Nagy, R.; Morioka, N.; Babin, C.; Erlekampf, J.; Berwian, P.; et al. Laser writing of scalable single color centers in silicon carbide. *Nano Lett.* **2019**, *19*, 2377−2383.

(16) Castelletto, S.; Maksimovic, J.; Katkus, T.; Ohshima, T.; Johnson, B. C.; Juodkazis, S. Color centers enabled by direct femtosecond laser writing in wide bandgap semiconductors. *Nanomaterials* **2021**, *11*, 72.

(17) Chen, Y.-C.; Salter, P. S.; Knauer, S.; Weng, L.; Frangeskou, A. C.; Stephen, C. J.; Ishmael, S. N.; Dolan, P. R.; Johnson, S.; Green, B. L.; et al. Laser writing of coherent colour centres in diamond. *Nat. Photonics* **2017**, *11*, 77−80.

(18) Chen, Y.-C.; Griffiths, B.; Weng, L.; Nicley, S. S.; Ishmael, S. N.; Lekhai, Y.; Johnson, S.; Stephen, C. J.; Green, B. L.; Morley, G. W.; et al. Laser writing of individual nitrogen-vacancy defects in diamond with near-unity yield. *Optica* **2019**, *6*, 662−667.

(19) Corrielli, G.; Crespi, A.; Osellame, R. Femtosecond laser micromachining for integrated quantum photonics. *Nanophotonics* **2021**, *10*, 3789−3812.

(20) Giakoumaki, A.; Coccia, G.; Bharadwaj, V.; Hadden, J.; Bennett, A.; Sotillo, B.; Yoshizaki, R.; Olivero, P.; Jedrkiewicz, O.; Ramponi, R. Quantum technologies in diamond enabled by laser processing. *Appl. Phys. Lett.* **2022**, *120*, 020502.

(21) Bharadwaj, V.; Jedrkiewicz, O.; Hadden, J.; Sotillo, B.; Vázquez, M. R.; Dentella, P.; Fernandez, T. T.; Chiappini, A.; Giakoumaki, A. N.; Le Phu, T.; et al. Femtosecond laser written photonic and microfluidic circuits in diamond. *Journal of Physics: Photonics* **2019**, *1*, 022001.

(22) Guo, X.; Delegan, N.; Karsch, J. C.; Li, Z.; Liu, T.; Shreiner, R.; Butcher, A.; Awschalom, D. D.; Heremans, F. J.; High, A. A. Tunable and transferable diamond membranes for integrated quantum technologies. *Nano Lett.* **2021**, *21*, 10392−10399.

(23) Guo, X.; Stramma, A. M.; Li, Z.; Roth, W. G.; Huang, B.; Jin, Y.; Parker, R. A.; Martínez, J. A.; Shofer, N.; Michaels, C. P.; et al. Microwave-Based Quantum Control and Coherence Protection of Tin-Vacancy Spin Qubits in a Strain-Tuned Diamond-Membrane Heterostructure. *Physical Review X* **2023**, *13*, 041037.

(24) Guo, X.; Xie, M.; Addhya, A.; Linder, A.; Zvi, U.; Deshmukh, T. D.; Liu, Y.; Hammock, I. N.; Li, Z.; DeVault, C. T. et al. Direct-bonded diamond membranes for heterogeneous quantum and electronic technologies. arXiv preprint arXiv:2306.04408, 2023.

(25) Kuruma, K.; Piracha, A. H.; Renaud, D.; Chia, C.; Sinclair, N.; Nadarajah, A.; Stacey, A.; Prawer, S.; Lončar, M. Telecommunication-wavelength two-dimensional photonic crystal cavities in a thin single-crystal diamond membrane. *Appl. Phys. Lett.* **2021**, *119*, 171106.

(26) Maletinsky, P.; Hong, S.; Grinolds, M. S.; Hausmann, B.; Lukin, M. D.; Walsworth, R. L.; Loncar, M.; Yacoby, A. A robust scanning diamond sensor for nanoscale imaging with single nitrogen-vacancy centres. *Nature Nanotechnol.* **2012**, *7*, 320−324.

(27) Losero, E.; Jagannath, S.; Pezzoli, M.; Goblot, V.; Babashah, H.; Lashuel, H. A.; Galland, C.; Quack, N. Neuronal growth on high-aspect-ratio diamond nanopillar arrays for biosensing applications. *Sci. Rep.* **2023**, *13*, 5909.

(28) Babinec, T. M.; Hausmann, B. J.; Khan, M.; Zhang, Y.; Maze, J. R.; Hemmer, P. R.; Lončar, M. A diamond nanowire single-photon source. *Nature Nanotechnol.* **2010**, *5*, 195−199.

(29) Hausmann, B. J.; Babinec, T. M.; Choy, J. T.; Hodges, J. S.; Hong, S.; Bulu, I.; Yacoby, A.; Lukin, M. D.; Lončar, M. Single-color centers implanted in diamond nanostructures. *New J. Phys.* **2011**, *13*, 045004.

(30) Andersen, S. K.; Bogdanov, S.; Makarova, O.; Xuan, Y.; Shalaginov, M. Y.; Boltasseva, A.; Bozhevolnyi, S. I.; Shalaev, V. M. Hybrid plasmonic bullseye antennas for efficient photon collection. *Acs Photonics* **2018**, *5*, 692−698.

(31) Li, L.; Chen, E. H.; Zheng, J.; Mouradian, S. L.; Dolde, F.; Schröder, T.; Karaveli, S.; Markham, M. L.; Twitchen, D. J.; Englund, D. Efficient photon collection from a nitrogen vacancy center in a circular bullseye grating. *Nano Lett.* **2015**, *15*, 1493−1497.

(32) Butcher, A.; High, A. A. All-dielectric multi-resonant bullseye antennas. *Opt. Express* **2022**, *30*, 12092−12103.

(33) Griffiths, B.; Kirkpatrick, A.; Nicley, S. S.; Patel, R. L.; Zajac, J. M.; Morley, G. W.; Booth, M. J.; Salter, P. S.; Smith, J. M. Microscopic processes during ultrafast laser generation of Frenkel defects in diamond. *Phys. Rev. B* **2021**, *104*, 174303.

(34) Day, A. M.; Dietz, J. R.; Sutula, M.; Yeh, M.; Hu, E. L. Laser writing of spin defects in nanophotonic cavities. *Nat. Mater.* **2023**, *22*, 696.

(35) Morelli, D.; Beetz, C.; Perry, T. Thermal conductivity of synthetic diamond films. *Journal of applied physics* **1988**, *64*, 3063−3066.

(36) Anufriev, R.; Wu, Y.; Ordonez-Miranda, J.; Nomura, M. Nanoscale limit of the thermal conductivity in crystalline silicon carbide membranes, nanowires, and phononic crystals. *NPG Asia Materials* **2022**, *14*, 35.

https://doi.org/10.1021/acs.nanolett.4c02639
Nano Lett. 2024, 24, 11224−11231

(37) Kurita, T.; Mineyuki, N.; Shimotsuma, Y.; Fujiwara, M.; Mizuochi, N.; Shimizu, M.; Miura, K. Efficient generation of nitrogen-vacancy center inside diamond with shortening of laser pulse duration. *Appl. Phys. Lett.* **2018**, *113*, 211102.
(38) Sotillo, B.; Bharadwaj, V.; Hadden, J.; Sakakura, M.; Chiappini, A.; Fernandez, T. T.; Longhi, S.; Jedrkiewicz, O.; Shimotsuma, Y.; Criante, L.; et al. Diamond photonics platform enabled by femtosecond laser writing. *Sci. Rep.* **2016**, *6*, 35566.
(39) Ajoy, A.; Bissbort, U.; Lukin, M. D.; Walsworth, R. L.; Cappellaro, P. Atomic-scale nuclear spin imaging using quantum-assisted sensors in diamond. *Physical Review X* **2015**, *5*, 011001.
(40) Li, P.-B.; Liu, Y.-C.; Gao, S.-Y.; Xiang, Z.-L.; Rabl, P.; Xiao, Y.-F.; Li, F.-L. Hybrid Quantum Device Based on N V Centers in Diamond Nanomechanical Resonators Plus Superconducting Waveguide Cavities. *Physical Review Applied* **2015**, *4*, 044003.
(41) Sangtawesin, S.; Dwyer, B. L.; Srinivasan, S.; Allred, J. J.; Rodgers, L. V.; De Greve, K.; Stacey, A.; Dontschuk, N.; O'Donnell, K. M.; Hu, D.; et al. Origins of diamond surface noise probed by correlating single-spin measurements with surface spectroscopy. *Physical Review X* **2019**, *9*, 031052.
(42) Ji, W.; Liu, Z.; Guo, Y.; Hu, Z.; Zhou, J.; Dai, S.; Chen, Y.; Yu, P.; Wang, M.; Xia, K.; et al. Correlated sensing with a solid-state quantum multisensor system for atomic-scale structural analysis. *Nat. Photonics* **2024**, *18*, 239.
(43) Sipahigil, A.; Evans, R. E.; Sukachev, D. D.; Burek, M. J.; Borregaard, J.; Bhaskar, M. K.; Nguyen, C. T.; Pacheco, J. L.; Atikian, H. A.; Meuwly, C.; et al. An integrated diamond nanophotonics platform for quantum-optical networks. *Science* **2016**, *354*, 847−850.
(44) Jia, Y.; Chen, F. Recent progress on femtosecond laser micro-/nano-fabrication of functional photonic structures in dielectric crystals: A brief review and perspective. *APL Photonics* **2023**, *8*, 090901.
(45) Gao, X.; Pandey, S.; Kianinia, M.; Ahn, J.; Ju, P.; Aharonovich, I.; Shivaram, N.; Li, T. Femtosecond laser writing of spin defects in hexagonal boron nitride. *ACS Photonics* **2021**, *8*, 994−1000.

https://doi.org/10.1021/acs.nanolett.4c02639
Nano Lett. 2024, 24, 11224−11231